Thin-Walled Composite Beams Under Bending, Torsional, and Extensional Loads

Ramesh Chandra,* Alan D. Stemple,† and Inderjit Chopra‡
University of Maryland, College Park, Maryland

Symmetric and antisymmetric layup graphite-epoxy composite beams with thin-walled rectangular cross sections are fabricated using an autoclave molding technique and tested under bending, torsional, and extensional loads. The bending slope and elastic twist at a station are measured using an optical system, and the results correlated with predicted values from a simple beam analysis as well as a refined finite element analysis. A symmetric ply layup results in bending-twist coupling whereas an antisymmetric layup causes extension-twist coupling. Simple analytical results with plane-stress assumption agree better with measured data as well as finite element predictions than with plane-strain assumption. For symmetric layup beams, the bending-induced twist and torsion-induced bending slope are predicted satisfactorily using simple analytical solution. Correlations with measured data, however, are generally improved using a finite element solution. For antisymmetric beams, axial force-induced twist is predicted satisfactorily by both methods.

Introduction

THIN-WALLED composite beams with closed and open cross sections are widely used in the construction of helicopter rotor blades. Through the control of lamination parameters (i.e., ply orientation and stacking sequence), structural couplings, such as bending-twisting and extension-twisting, are introduced. Traditionally, the couplings used in helicopter rotors are introduced by mechanical means. Recent studies[1-3] have shown that these elastic couplings have a powerful influence on blade dynamics, including aeroelastic stability, vibration, dynamic stresses, and loads. Currently, composite blades are built as symmetric and balanced structures such that these elastic couplings are completely eliminated. With the availability of a structural analysis that can accurately model the couplings associated with composite materials, the potential benefits of structural couplings can be realized by the rotorcraft industry.

The objectives of this paper are to experimentally identify the static characteristics (including structural couplings) of thin-walled composite box beams and to correlate these with analytical predictions. Simple single-cell closed-section slender beams are built out of graphite-epoxy laminae and tested under bending, torsional, and extensional loads.

Two categories of thin-walled composite beams are investigated and referred to as the symmetric and antisymmetric configurations. In a symmetric configuration, the ply layups on opposite flanges are mirror images with respect to the midaxis, whereas for an antisymmetric configuration, the ply layups on opposite flanges are of reversed orientation. As discussed in Ref. 1, the symmetric layup beams result in bending-twisting structural couplings, whereas antisymmetric beams cause extension-twisting structural couplings. Bending-twisting structural couplings are similar to the classical pitch-flap and pitch-lag couplings in helicopter rotor blades, whereas the extension-twisting couplings are somewhat unique in nature. By placing plies with a specific layup, the desired structural couplings can be achieved.

Received April 25, 1989; revision received Jan. 4, 1990. Copyright © 1990 by the American Institute of Aeronautics and Astronautics, Inc. All rights reserved.

*Research Associate, Department of Aerospace Engineering.

†Rotorcraft Fellow, Department of Aerospace Engineering; currently Engineer, McDonnell Douglas Helicopter Company, Mesa, AZ.

‡Professor and Acting Chairman, Department of Aerospace Engineering. Associate Fellow AIAA.

For the analysis of thin-walled composite beams, nonclassical effects, such as cross-sectional warping and transverse shear deflections, become important. Many analyses have been formulated to analyze composite beams with varying levels of assumptions and idealization for these nonclassical effects. In Refs. 1 and 2, Hong and Chopra developed a nonlinear analysis for thin-walled composite beams undergoing transverse bending (flap and lag), torsion, and axial deflections. Cross-sectional warping was expressed in terms of a simple analytical expression. The effects of transverse shear were, however, neglected for thin-walled beams. Important structural coupling terms caused by ply orientations were identified, and their effect on blade stability was investigated extensively. Through beneficial structural couplings, the potential of composite tailoring of rotor blades to minimize blade stresses and vibration and to maximize aeroelastic stability was shown in Ref. 3. Recently, Stemple and Lee[4] developed a refined finite element analysis for composite beams in which the cross-sectional warping and transverse shear were included in a unified and consistent manner. This analysis was validated extensively with a shell finite element analysis for several beam configurations. Rehfield[5] presented a simple linear composite beam analysis in which the cross-sectional warping was expressed in a simple analytical expression (as in Ref. 2), and the effect of transverse shear was also included. Additional couplings due to shear were identified: bending-shear coupling for an antisymmetric layup beam and extension-shear coupling for a symmetric layup beam. That analysis assumed a uniform strain across the wall thickness, and also, the formulation was developed for a cross section with uniform thickness. There are other papers[6,7] that have also addressed the modeling of composite blades. For a general discussion on the limitation of different analyses, see a recent review paper.[8]

There have been some selected attempts to obtain experimental data for thin-walled composite beams under static loading. At the University of Maryland, Schwiesow[9] built thin-walled rectangular cross-section composite beams using an autoclave molding technique. Symmetric and antisymmetric beams were fabricated out of graphite-epoxy prepreg tape. Plies were wrapped around an aluminum mandrel (two tapered beams) enclosed in a vacuum bag and cured in an autoclave. A tensile test machine was used to remove the mandrel from the cured beam. The resulting specimens were of poor quality because of the formation of ridges on the surface, but the proper structural couplings were identified. Later on, Salzberg[10] built thin-walled rectangular cross section

composite beams using a thermal expansion process. Graphite-epoxy prepreg was wrapped around an elastomer mandrel with a high coefficient of thermal expansion, enclosed by an aluminum clam shell and then cured in an autoclave. The pressure for curing was generated by the thermal expansion of the elastomer. Symmetric and antisymmetric layup thin-walled beams of high quality were built. The correlation of predicted and measured static characteristics, including structural couplings, however, was less than satisfactory and was attributed to an excessive resin content in the fabricated beams. In the present research, the problems associated with these two approaches are solved, and thin-walled composite beams of good quality are built using an autoclave molding technique.

At NASA Langley, Nixon[11] successfully built thin circular composite tubes of antisymmetric layup from graphite-epoxy laminae. By wrapping the same laminae all over the circumference, beams of uniform thickness were fabricated. Torsion and axial tension tests were performed using a testing machine. Measured data were correlated satisfactorily (within 11%) with calculated results obtained using composite beam analysis of Rehfield[5] as well as with shell finite-element analysis.[12] Measured nonrotating vibration characteristics were also correlated satisfactorily (within 13%) with analytical predictions.

In the present investigation, composite beams with specialized characteristics are built to validate the theory. Thin-walled rectangular-section beams were built out of graphite-epoxy prepregs, which represent either symmetric or antisymmetric configurations, and the characteristics are not identical for all four laminates (non-uniform thickness). Static structural characteristics are identified experimentally for these beams under bending, torsion, and extensional loads. Measured results are correlated with analytical predictions.

Analyses

Simplified Composite Beam Analysis

Following the coupled nonlinear analysis of Hong and Chopra[1] for a composite blade undergoing flap bending, lag bending, elastic twist, and axial deflections, a simplified linear analysis is derived for bending and torsion of thin-walled symmetric composite beams

$$\begin{Bmatrix} M \\ T \end{Bmatrix} = \begin{bmatrix} EI & K_{P_s} \\ K_{P_s} & GJ \end{bmatrix} \begin{Bmatrix} w'' \\ \phi' \end{Bmatrix} \tag{1}$$

where M and T, respectively, are the bending moment and torque at a given beam location, EI is the effective flap bending stiffness, GJ is the effective torsional stiffness, K_{P_s} is the bending-twisting structural coupling, w'' or d^2w/dx^2 is the bending curvature, and ϕ' or $d\phi/dx$ is the twist derivative.

In a similar way, following Ref. 1, the simplified linear analysis for extension and torsion of thin-walled antisymmetric beams is derived as

$$\begin{Bmatrix} T \\ F \end{Bmatrix} = \begin{bmatrix} GJ & K_{P_a} \\ K_{P_a} & EA \end{bmatrix} \begin{Bmatrix} \phi' \\ u' \end{Bmatrix} \tag{2}$$

where F is the axial force, EA is the effective extensional stiffness, K_{P_a} is the extension-twisting structural coupling, and u' or du/dx is the axial deflection derivative. The structural constants EI, GJ, EA, K_{P_s}, and K_{P_a} are defined in the Appendix. The structural coupling K_{P_s} becomes zero for antisymmetric configurations whereas K_{P_a} becomes zero for symmetric beams. The effects of cross-sectional warping due to torsion are included in an approximate manner.[1] The effects of transverse shear are neglected, however, for these simplified derivations.

In this analysis, four sides of the box beam are modeled as general composite laminates. The terminology that is used to describe symmetric and antisymmetric solid sections is extended to hollow section (box beam). No approximation of uniform strain across the wall thickness is made.

The bending slope and bending-induced twist in a uniform cantilevered symmetric beam subjected to a tip load P are obtained by using Eq. (1) as

$$w_{,x} = \frac{P}{2(EI - K_{P_s}^2/GJ)}(2lx - x^2) \tag{3}$$

$$\phi = \frac{K_{P_s}/GJ}{2(EI - K_{P_s}^2/GJ)} P(2lx - x^2) \tag{4}$$

The twist and torsion-induced bending slope in a cantilevered symmetric beam subjected to tip torsion load T are also obtained by using Eq. (1) as

$$\phi = \frac{T}{(GJ - K_{P_s}^2/EI)} x \tag{5}$$

$$w_{,x} = -\frac{K_{P_s}/EI}{(GJ - K_{P_s}^2/EI)} Tx \tag{6}$$

The twist in an antisymmetric beam subjected to torsional and extensional loads at the tip, T and F, respectively, is obtained using Eq. (2) as

$$\phi = \frac{T}{(GJ - K_{P_a}^2/EA)} x \tag{7}$$

$$\phi = -\frac{(K_{P_a}/EA)}{(GJ - K_{P_a}^2/EA)} Fx \tag{8}$$

where x is the spanwise distance from root and l is the total length of the beam. Results using these equations are denoted as analytical results in the graphs presented in this paper.

Finite Element Beam Analysis

Recently, Stemple and Lee[4] developed a refined finite element analysis to model thin-walled composite beams with complicated cross sections, tapers, twist, and arbitrary planforms. This formulation uses a shear flexible beam element with warping displacements parallel to the deformed beam axis superimposed over the cross section and is capable of handling the combined bending, torsional, and extensional behavior of composite beams. The beam element has two types of nodes, translational and rotational and warping. Each translational and rotational node has three translational degrees of freedom and three rotational degrees of freedom whereas each warping node has a single translational degree of freedom, which is parallel to the deformed beam axis. In this formulation, the cross-sectional warping associated with torsion as well as bending is included in a unified and consistent manner. For thin-walled beams, the strain is assumed to vary linearly through the wall thickness. This beam formulation has the accuracy of more elaborate shell and solid element formulation and is extremely efficient because of the relatively small number of degrees of freedom required.

Experiment

Fabrication of Box Beam

An autoclave molding technique is employed to fabricate graphite-epoxy thin-walled box beams. Graphite-epoxy unidirectional prepregs (AS4/3501-6 from Hercules) are laid up on a split metal mold. The mold has a 1/16-in. radius at its corners. This curvature is needed to avoid sharp corners and also to ensure tight wrap of the prepreg layers. Prepreg layers are cut to the desired size using templates. For symmetric angle ply beams, each layer has two joints, which are intentionally staggered for better strength. The layers in antisymmetric beams have only one joint for each ply.

The mold is first given three coats of releasing agent (All release 30, Air Tech International). Mild heating with the help

Table 1 Details of composite beams

Configuration	Flanges		Webs		EI lb in.^{2} 10^3	GJ lb in.^{2} 10^3	K_{P_s} lb in.^{2} 10^3	EA lb 10^3	K_{Pa} lb in. 10^3
	Top	Bottom	Left	Right					
Symmetric 1	$[0/90]_3$	$[0/90]_3$	$[0/90]_3$	$[0/90]_3$	45	8	0	—	0
Symmetric 2	$[15]_6$	$[15]_6$	$[15/-15]_3$	$[15/-15]_3$	77	18	20	—	0
Symmetric 3	$[30]_6$	$[30]_6$	$[30/-30]_3$	$[30/-30]_3$	54	38	29	—	0
Symmetric 4	$[45]_6$	$[45]_6$	$[45/-45]_3$	$[45/-45]_3$	28	49	23	—	0
Antisymmetric 1	$[15]_6$	$[-15]_6$	$[15]_6$	$[-15]_6$	—	18	0	1582	122
Antisymmetric 2	$[0/30]_3$	$[0/-30]_3$	$[0/30]_3$	$[0/-30]_3$	—	24	0	1436	87
Antisymmetric 3	$[0/45]_3$	$[0/-45]_3$	$[0/45]_3$	$[0/-45]_3$	—	29	0	1179	69

Geometry of Beam: thin-walled rectangular cross section; length = 36 in., width = 0.953 in., depth – 0.53, in.; ply thickness = 0.005 in., number of plies = 6, wall thickness = 0.030 in. Mechanical Properties: $E_L = 20.59 \times 10^6$ apsi., $E_T = 1.42 \times 10^6$ psi., $G_{LT} = 0.89 \times 10^6$ psi., $\mu_{LT} = 0.42$[15]

of a hair dryer is used for the layup of the first lamina onto the mold. A vacuum pump is used in the further compaction of this layer. After laminating the desired number of plies, peel ply is wrapped to provide the surface finish of the beam. Depending upon the desired resin content in the cured composite beam, a number of bleeder and breather layers are then applied. For the present work, three layers of these are used to yield a fiber volume fraction of 65% in the beam.

The layup is cured in a microprocessor-controlled autoclave. The cure cycle given by the prepreg manufacturer is used. At the end of the cure, the layup is removed from the autoclave. The vacuum bag, bleeder, breather, and release plies were removed, and the beam is released from the mold. Thus, composite box beams with a length of 36 in. and a length/depth ratio of 56 are built. Table 1 shows the configuration of symmetric and antisymmetric beams.

In antisymmetric beams, initial twist of the order of 5–10 deg due to curing stresses was noticed. In fact, the initial twist created much difficulty in the release of beams from the mold for $[30]_6$ and $[45]_6$ configurations and, hence, they were shelved. Instead $[0/30]_3$ and $[0/45]_3$ beams were fabricated where initial twist due to curing was small.

Testing

Figure 1 shows a schematic diagram of the test stand wherein the bending, torsional, and extensional loads are applied to the cantilevered composite beams. These beams are clamped by means of stiff plates and six bolts. To ensure the clamped condition of zero bending deflection, zero bending slope and zero warping displacements, a metallic insert is used in the clamped part, and the bolts are uniformly tightened with the help of a torque wrench to 60% of maximum allowable torque. While testing antisymmetric beams in tension, the loading end is permitted to twist by means of a special end fixture with a thrust bearing. The beam's bending slope and twist at a particular spanwise station are measured using an optical system. A light beam is reflected from mirrors attached on the surface of the beam onto a vertical screen or wall. The slope is determined by the amount that the light is deflected.

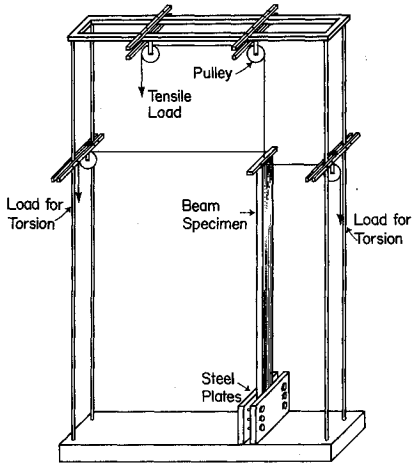

Fig. 1 Schematic of test setup.

The bending slope is calculated from $w_{,x} = (\delta z/2d)$ where δz is the vertical movement of the laser point and d is the distance between the mirror and the screen. In a similar way, twist at a station can be determined from the horizontal movement of the laser point, δ_y, $\phi = (\delta_y/2d)$.

To measure spanwise variation of bending slope and twist, six or seven mirrors with a diameter of 0.32 in. are mounted at different stations along the beam. First, the beam specimens were aligned, and then loads were applied.

Results and Discussion

In order to validate the test procedure, a bending test was conducted on an aluminum beam with a solid rectangular cross section. The beam had a length of 29 in., a width of 1 in., and a depth or thickness of 0.375 in. This produces a length/depth ratio of 78. There was an excellent correlation between analytical and experimental results.

Using this test setup, static tests were conducted on composite beams of different configurations as described in Table 1. For each configuration, two identical specimens were built and each test was repeated two or three times on each beam. Thus, reliable data on the static characteristics of these beams are generated. Table 1 shows the calculated values of bending stiffness EI, torsion stiffness GJ, bending-twist coupling stiffness K_{P_s} for symmetric beams, the calculated values of extensional stiffness EA, torsional stiffness GJ, and extension-twist coupling stiffness K_{P_a} for the antisymmetric beams.

The experimental data on bending slopes and twists were compared with the theoretical results obtained using the simple analysis [Eqs. (3–8)] and the finite element analysis described in Ref. 4. In order to select the suitable mesh for the finite element method, a convergence study was conducted. For example, six different meshes with 2 and 3 elements along the span and 8, 12, and 14 elements in the cross section were examined for the analysis of a $[45]_6$ symmetric beam under bending load. It was determined that (2×12) mesh yielded converged results, and hence this mesh was used for the analyses of all other symmetric and antisymmetric beams. Also, the influence of constrained warping was investigated by carrying out this analysis with and without suppressing the warping degree of freedom at the clamped end of the beam. The difference in the results for these two cases was found to be small. This may be due to a high slenderness ratio and the special layup adopted in these beams.

Bending of Symmetric Beam

Figure 2 shows the bending slope distribution for the $[0/90]_3$ composite beams under a 1-lb tip load. For this symmetric configuration, plies of 0 and 90 deg are aligned in the spanwise direction and therefore introduce no bending-twisting structural coupling. Good correlation exists between experimental data and predicted results obtained by both analyses for this

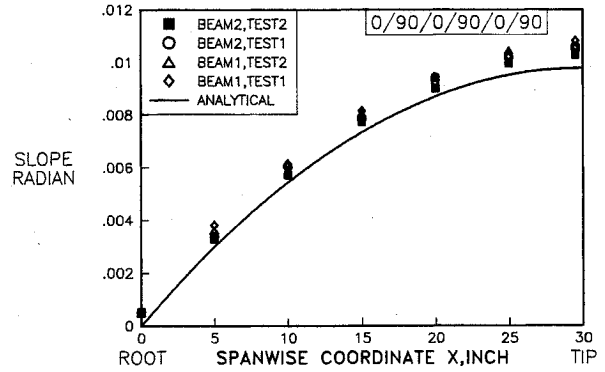

Fig. 2 Bending slope of $[0/90]_3$ beam under 1 lb bending load at tip.

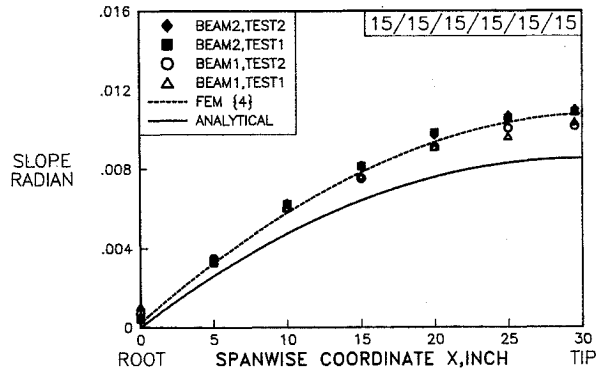

Fig. 3 Bending slope of $[15]_6$ symmetric beam under 1 lb bending load at tip.

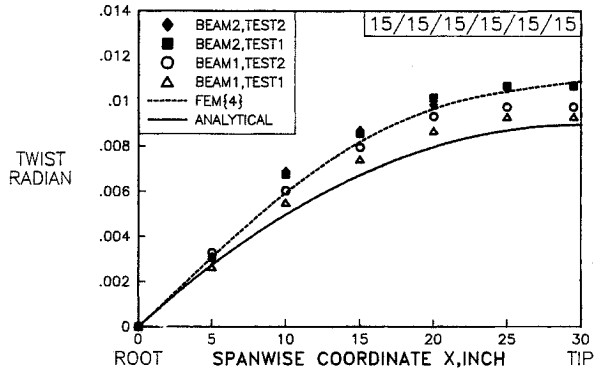

Fig. 4 Bending-induced twist of $[15]_6$ symmetric beam under 1 lb bending load at tip.

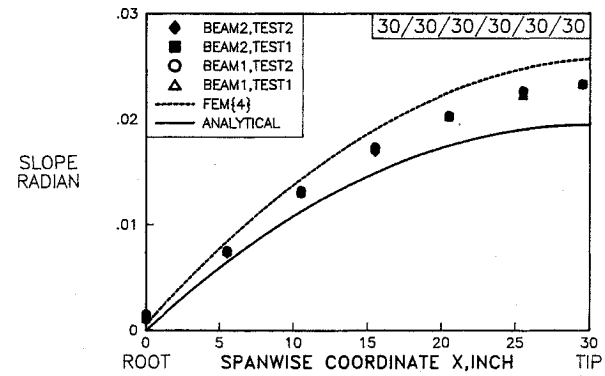

Fig. 5 Bending slope of $[30]_6$ symmetric beam under 1 lb bending load at tip.

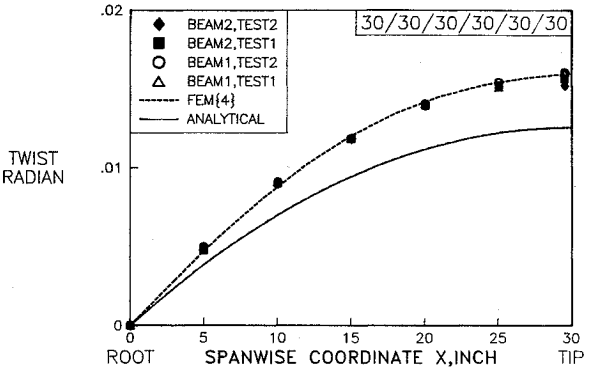

Fig. 6 Bending-induced twist of $[30]_6$ symmetric beam under 1 lb bending load at tip.

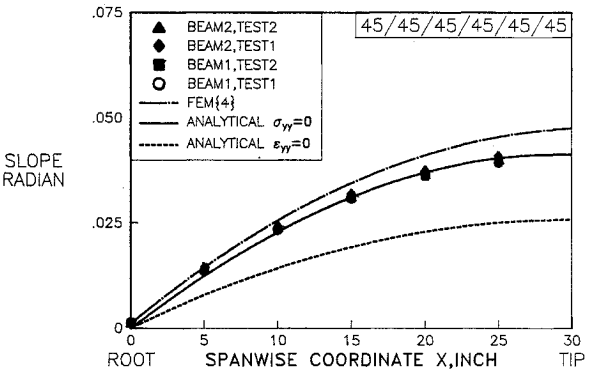

Fig. 7 Bending slope of $[45]_6$ symmetric beam under 1 lb bending load at tip.

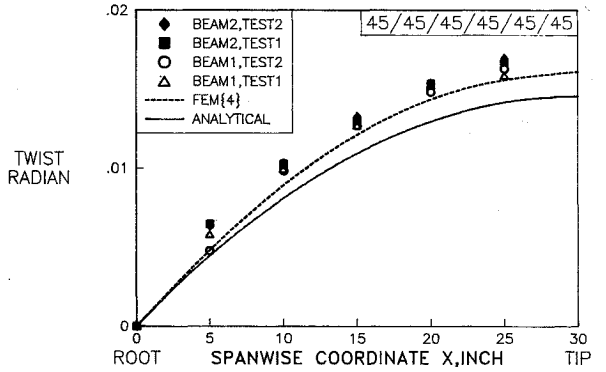

Fig. 8 Bending-induced twist of $[45]_6$ symmetric beam under 1 lb bending load at tip.

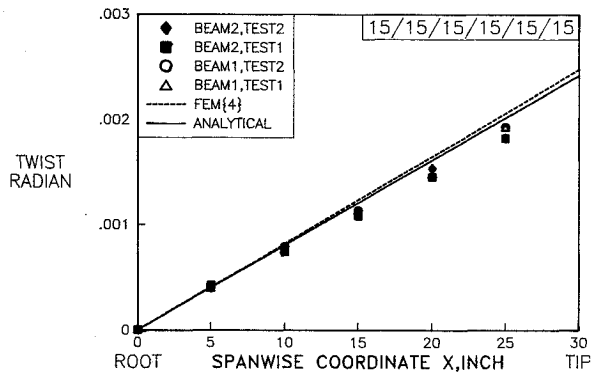

Fig. 9 Twist of $[15]_6$ symmetric beam under 1 in.-lb torsional moment at tip.

configuration. It is interesting to note that results from the simple approximate analysis and the finite element analysis cannot be distinguished from each other in Fig. 2, and hence the finite element results are not included in this figure. This indicates that the effects of warping and transverse shear are quite small for this configuration.

Figures 3 and 4, respectively, present bending slope and bending-induced twist for the $[15]_6$ composite beams under a tip load of 1 lb. For this symmetric configuration, the ply layup introduces bending-twist structural coupling. The finite element bending slope results correlate better with measured data than analytical results. For this configuration, transverse shear appears important, which is evident from the finite-slope value at blade root calculated using the finite element approach. For the bending-induced twist, both results fall within the scatter of data.

Figures 5 and 6, respectively, show bending slope and elastic twist for the $[30]_6$ composite beams under a 1-lb tip load. For bending slope, there are considerable differences between finite element results and analytical results; however, neither one appears better in terms of correlation with the experimental data. For bending-induced twist, the finite element results agree much better with measured data than analytical results. This may be pointing to a deficiency in the modeling of warping and transverse shear in the analytical approximations.

Figures 7 and 8 present results for the $[45]_6$ symmetric composite beams. There are some differences between finite element results and analytical approximations for both bending slope and induced twist distributions. For bending slope, two types of simple analytical results are presented—the first one using plane-stress assumption ($\sigma_{yy} = 0$) and the second one using plane-strain assumption ($\epsilon_{yy} = 0$). There is no doubt that the results with the plane-stress assumption agree better with the experimental data and the finite element results than the results with the plane-strain assumption. In all earlier as well as subsequent results, analytical results with only plane-stress assumption are presented.

For bending-induced twist, agreement between the finite element results and the measured data is very good (lie within scatter of data). Analytical results, however, underestimate magnitudes but lie within 15% of measured values. Estimated bending-induced slopes by both methods generally agree well with measured values (within 12%), and some of the differences may be attributed to the structural constants (manufacturer supplied values are used). The bending-induced slope increases considerably when ply angles are increased, whereas the bending-induced twist increases less dramatically with higher ply angles.

Torsion of Symmetric Beams

Figures 9 and 10 present the twist and torsion-induced bending-slope distributions for the $[15]_6$ beams under unit torsional load at the tip. It is interesting to note from Fig. 9 that the experimental, analytical, and finite element method values of twist are quite close to each other. This indicates that the torsional warping representation in the analytical derivation is adequate for this configuration of beam. However, the analytical and finite element values of torsion-induced bending slope differ somewhat from each other, although this difference is within the scatter of the experimental values as shown in Fig. 10. Figures 11 and 12 show the twist and bending-slope distributions for the $[30]_6$ beams. Excellent correlation between experimental and calculated values of twist is seen in Fig. 11. For the torsion-induced bending slope, the analytical results agree better with measured data than the finite element results. A good correlation between experimental and finite element results for twist and bending slope is seen for the $[45]_6$ beams in Figs. 13 and 14. For these beams, the elastic twist decreases and the torsion-induced slope increases with higher ply angles.

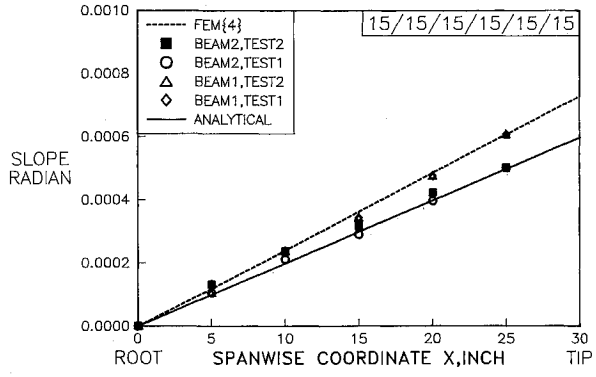

Fig. 10 Torsion-induced bending slope of $[15]_6$ symmetric beam under 1 in.-lb torsional moment at tip.

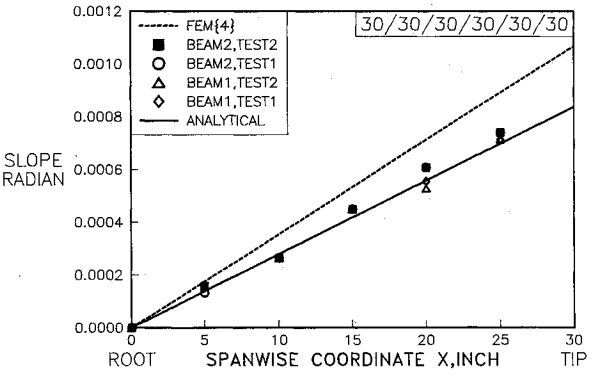

Fig. 12 Torsion-induced bending slope of $[30]_6$ symmetric beam under 1 in.-lb torsional moment at tip

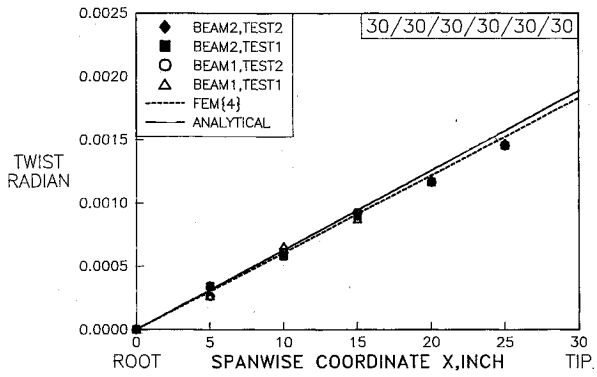

Fig. 11 Twist of $[30]_6$ symmetric beam under 1 in.-lb torsional moment at tip.

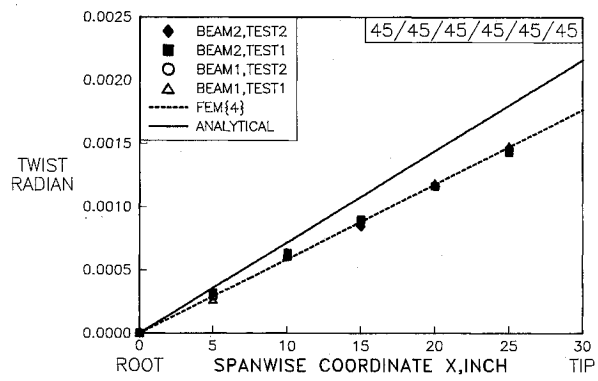

Fig. 13 Twist of $[45]_6$ symmetric beam under 1 in.-lb torsional moment at tip.

Calculated results from both methods generally correlate with measured data (within 15%).

Torsion and Extension of Antisymmetric Beams

Figure 15 shows the twist distribution for the $[15]_6$ antisymmetric beams subjected to a unit torsional load at the tip. Analytical and finite element estimations of twist are quite close to each other and are within the scatter of the experimental data. This reveals that the representation of torsional warping in the analytical derivation is adequate for this configuration. The spanwise twist variation for this beam subjected to unit extensional load is shown in Fig. 16. Finite element results (both) with experimental data is not as good, particularly near the tip. This finding is plausible due to the fact that the local state of stress due to loading does not quickly decay in graphite-epoxy material.[14]

Figure 17 shows the twist distribution for the $[0/30]_3$ beams under a unit torsional load at the tip. Analytically predicted values of twist agree better with experimental data than the finite element prediction. However, differences between these computed results are generally small. Figure 18 shows the spanwise variation of twist in the $[0/30]_3$ beams due to a unit tensile load. Both calculated results are identical and correlate well with experimental data. Figure 19 illustrates the twist distribution in the $[0/45]_3$ beams subjected to a unit torsional lead. Again, the calculated twist values using simple analytical expression agree better with experimental data than finite element values. Figure 20 shows the twist variation in $[0/45]_3$ beam due to the unit tensile load. Here, again, we notice a good correlation between calculated and experimental twist except towards the loading end. It is to be noted from Figs. 17-20 that the correlation between the experimental and calcu-

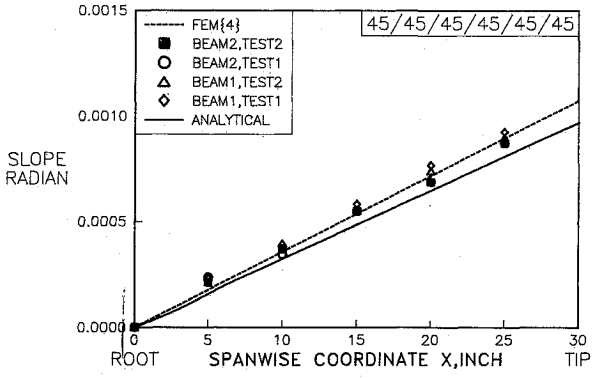

Fig. 14 Torsion-induced bending slope of $[45]_6$ symmetric beam under 1 in.-lb torsional moment at tip.

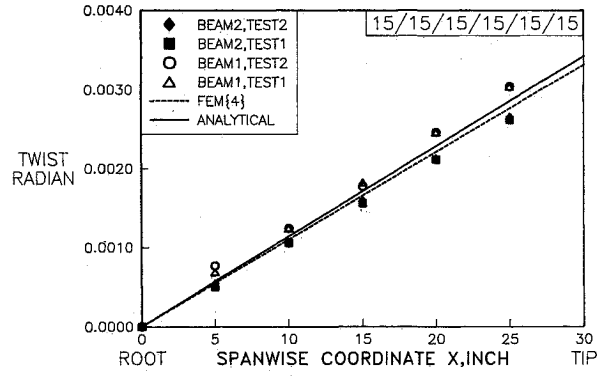

Fig. 15 Twist of $[15]_6$ antisymmetric beam under 1 in.-lb torsional moment at tip.

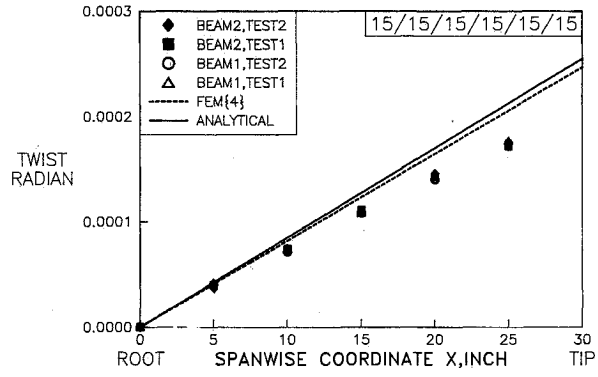

Fig. 16 Extension-induced twist of $[15]_6$ antisymmetric beam under 1-lb tensile load.

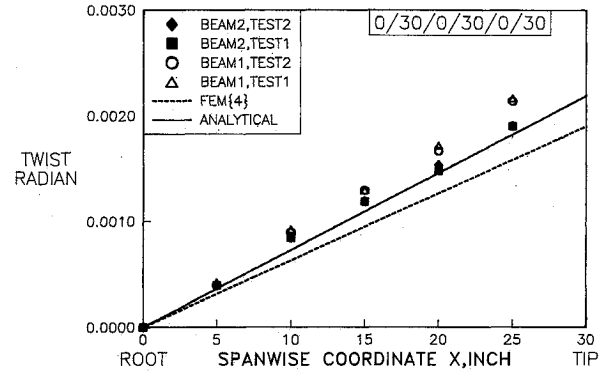

Fig. 17 Twist of $[0/30]_3$ antisymmetric beam under 1 in.-lb torsional moment at tip.

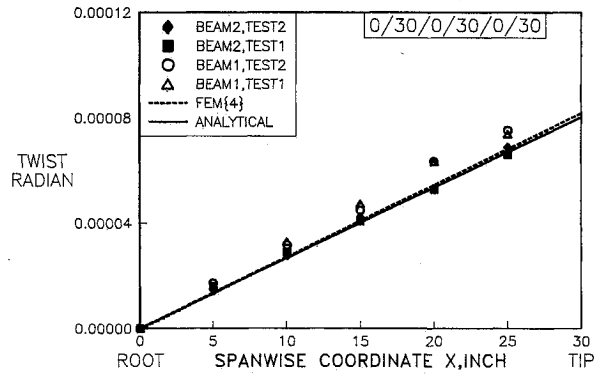

Fig. 18 Extension-induced twist of $[0/30]_3$ antisymmetric beam under 1-lb tensile load.

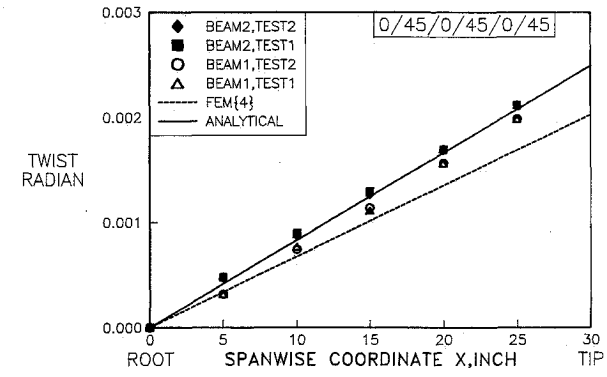

Fig. 19 Twist of $[0/45]_3$ antisymmetric beam under 1 in.-lb torsional moment at tip.

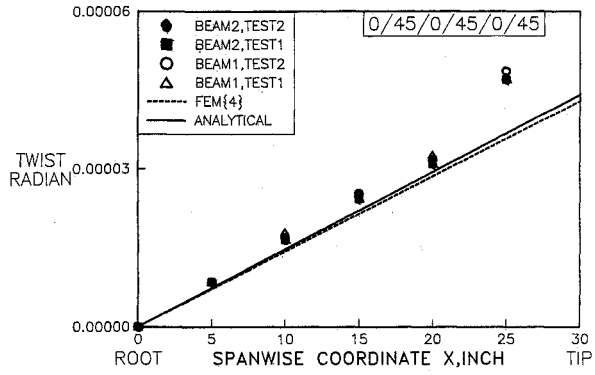

Fig. 20 Extension-induced twist of $[0/45]_3$ antisymmetric beam under 1-lb tensile load.

lated results is generally quite good, and there are small differences between these two calculated results. Torsion-induced twist as well as axial force-induced twist decrease with higher ply angles.

Conclusions

Using an autoclave molding technique, thin-walled rectangular cross-section composite beam specimens of very good quality were built out of graphite-epoxy prepreg material. Reliable static test data on the bending slope and twist were achieved for symmetric and antisymmetric beams using a simple test setup and a laser optical system. Measured static structural data were correlated with results from a simple analytical approximation as well as with a refined finite element analysis.

Based on this study, the following conclusions are drawn:

1) Symmetric layup composite beams result in bending-twist structural coupling. Bending-induced slopes increase with higher ply angles, and values predicted by both methods generally correlate satisfactorily with measured data (with 12%). Bending-induced twist increases with higher ply angles and finite element predictions show excellent correlation with measured data (within the scatter of data). Analytical predictions underestimate bending-induced twist but are within 15% of measured values.

2) For symmetric layup beams with higher ply angles, torsion-induced twist decreases and torsional-induced slope increases. Calculated results by both methods agree well with measured data (within 15%).

3) Simple analytical results with plane-stress assumption agree better with measured data and finite element results than with plane-strain assumption.

4) Antisymmetric layup beams result in extension-twist structural coupling. Torsion-induced twist as well as axial force-induced twist decrease with higher ply angles, and results predicted by both methods generally correlate very satisfactorily with measured data. Some differences in correlation at the tip may be attributed to the simulation of loading condition in the experiment.

Appendix

Stiffness Coefficients: EI, GJ, K_{P_s}, EA, and K_{P_a}

$$EI = \sum_{k=1}^{N} \iint_{1,2} \bar{C}_{11}^{(k)} \zeta^2 d\eta d\zeta + \sum_{l=1}^{M} \iint_{3,4} \bar{C}_{11}^{(l)} \zeta^2 d\eta d\zeta$$

$$GJ = \sum_{k=1}^{N} \iint_{1,2} \bar{C}_{66}^{(k)} \zeta^2 d\eta d\zeta + \sum_{l=1}^{M} \iint_{3,4} \bar{C}_{66}^{(k)} \hat{\eta}^2 d\eta d\zeta$$

$$K_{P_s} = \sum_{k=1}^{N} \iint_{1,2} \bar{C}_{16}^{(k)} \hat{\zeta} \zeta d\eta d\zeta$$

$$EA = \sum_{k=1}^{N} \iint_{1,2} \bar{C}_{11}^{(k)} d\eta d\zeta + \sum_{l=1}^{M} \iint_{3,4} \bar{C}_{11}^{(l)} d\eta d\zeta$$

$$K_{P_a} = -\sum_{k=1}^{N} \iint_{1} \bar{C}_{16}^{(k)} \hat{\zeta} d\eta d\zeta + \sum_{k=1}^{N} \iint_{2} \bar{C}_{16}^{(k)} \zeta d\eta d\zeta + \sum_{l=1}^{M} \iint_{3} \bar{C}_{16}^{(l)} \hat{\eta} d\eta d\zeta - \sum_{l=1}^{M} \iint_{4} \bar{C}_{16}^{(l)} \hat{\eta} d\eta d\zeta$$

(1,2, respectively, represent top and bottom laminates of box beam; 3,4, respectively, represent left and right side laminates of box beam), where

$\bar{C}_{11} = \bar{Q}_{11} - \bar{Q}_{12}^2/\bar{Q}_{22}$
$\bar{C}_{16} = \bar{Q}_{16} - \bar{Q}_{12} \times \bar{Q}_{26}/\bar{Q}_{22}$
$\bar{C}_{66} = \bar{Q}_{66} - \bar{Q}_{26}^2/\bar{Q}_{22}$
$\bar{Q}$ = stiffness matrix of kth lamina in $x-\eta$ or $x-\zeta$ plane (Fig. 4 of Ref. 1)
N = number of layers in laminate 1 or 2
M = number of layers in laminate 3 or 4
η, ζ = coordinates in the plane of cross section
$\hat{\zeta} = \zeta + \lambda, \eta$
$\hat{\eta} = \eta - \lambda, \zeta$
λ = warping function

Assumed warping function = $\beta\zeta\eta$

$\beta = (c-d)/(c+d)$ for uniform wall thickness of the cross section
c = width of beam
d = depth of beam

Acknowledgments

This research work was supported by Army Aerostructures Directorate, Grant NAG-1-853; Technical Monitor was Mark W. Nixon.

References

[1]Hong, C. H., and Chopra, I., "Aeroelastic Stability of a Composite Blade," *Journal of the American Helicopter Society*, Vol. 30, No. 2, 1985, pp. 57-67.

[2]Hong, C. H., and Chopra, I., "Aeroelastic Stability Analysis of a Composite Bearingless Rotor Blade," *Journal of the American Helicopter Society*, Vol. 31, No. 4, 1986, pp. 29-35.

[3]Panda, B., and Chopra, I., "Dynamics of Composite Rotor Blades in Forward Flight," *Vertical*, Vol. 11, No. 1/2, 1987, pp. 187-209.

[4]Stemple, A. D., and Lee, S. W., "A Finite Element Model for Composite Beams with Arbitrary Cross-Sectional Warping," *AIAA Journal*, Vol. 26, No. 12, 1988.

[5]Rehfield, L. W., "Design Analysis Methodology for Composite Rotor Blades," Air Force Wright Aeronautical Lab, Wright-Patterson AFB, OH, AFWAL-TR-85-3094, June 1985.

[6]Bauchau, O. A., and Hong, C. H., "Large Displacement Analysis of Naturally Curved and Twisted Composite Beams," *AIAA Journal*, Vol. 25, No. 11, 1987, pp. 1469-1475.

[7]Kosmatka, J. B., and Friedmann, P. P.. "Structural Dynamic Modeling of Advanced Composite Propellers by the Finite Element Method," *Proceedings of the 28th AIAA/ASME/ASCE/AHS Structures, Structural Dynamics and Material Conference*, AIAA, Washington, DC, April 1987.

[8]Hodges, D. H., "A Review of Composite Rotor Blade Modeling," *Proceedings of the 29th AIAA/ASME/ASCE/AHS Structures, Structural Dynamics and Materials Conference*, AIAA, Washington, DC, April 1988.

[9]Schwiesow, B. R., "Experimental Identification of Stiffness Coupling Terms in a Composite Beam," M. S. Thesis, Dept. of Aerospace Engineering, Univ. of Maryland, July 1985.

[10]Salzberg, A., "Experimental Identification of Stiffness Coupling

Terms in Composite Box Beams Manufactured by Thermal Expansion," M. S. Thesis, Dept. of Aerospace Engineering, Univ. of Maryland, Dec. 1986.

[11]Nixon, M. W., "Extension-Twist Coupling of Composite Circular Tubes with Application to Tilt Rotor Blade Design," *Proceedings of the 28th AIAA/ASME/ASCE/AHS Structures, Structural Dynamics and Materials Conference*, AIAA, Washington, DC, April 1987.

[12]Hodges, R. V., Nixon, M. W., and Rehfield, L. W., "Comparison of Composite Rotor Blade Models: A Coupled-Beam Analysis and an MSC/NASTRAN Finite-Element Model," NASA TM-89024, 1987.

[13]Hong, C., and Chopra, I., "Aeroelastic Stability Analysis of a Composite Blade," *40th Annual Forum of the American Helicopter Society*, Crystal City, VA, May 1984.

[14]Choi, I., and Horgan, C. O., "Saint-Venant's Principle and End Effects in Anisotropic Elasticity," *Journal of Applied Mechanics*, Vol. 44, Sept. 1977, pp. 424–430.

[15]"AS/3501-6 Material Properties," Technology Lab. for Advanced Composites, MIT, Cambridge, MA, internal report, 1986.

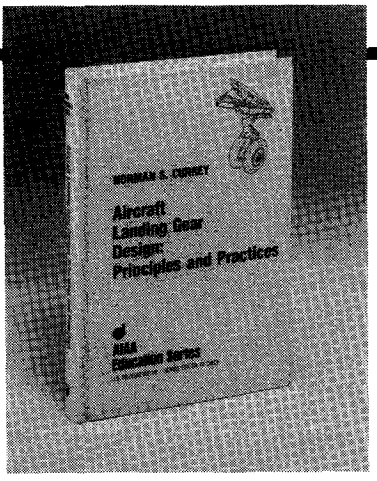

Aircraft Landing Gear Design:
Principles and Practices

by Norman S. Currey

The only book available today that covers military and commercial aircraft landing gear design. It is a comprehensive text that leads the reader from the initial concepts of landing gear design right through to final detail design. The text is backed up by calculations, specifications, references, working examples, and nearly 300 illustrations!

This book will serve both students and engineers. It provides a vital link in landing gear design technology from historical practices to modern design trends. In addition, it considers the necessary airfield interface with landing gear design.

To Order, Write, Phone, or FAX:

AIAA

c/o TASCO, 9 Jay Gould Ct., P.O. Box 753
Waldorf, MD 20604 Phone (301) 645-5643
Dept. 415 ■ FAX (301) 843-0159

AIAA Education Series
1988 373pp. Hardback
ISBN 0-930403-41-X

AIAA Members $42.95
Nonmembers $52.95
Order Number: 41-X

Postage and handling $4.75 for 1-4 books (call for rates for higher quantities). Sales tax: CA residents 7%, DC residents 6%. Orders under $50 must be prepaid. Foreign orders must be prepaid. Please allow 4 weeks for delivery. Prices are subject to change without notice.

945